Journal of Advanced Ceramics
2020, **9**(1): 45–54
https://doi.org/10.1007/s40145-019-0346-0
ISSN 2226-4108
CN 10-1154/TQ

Research Article

Red-emitting YAG:Ce,Mn transparent ceramics for warm WLEDs application

Junrong LING[a,b], Youfu ZHOU[a,*], Wentao XU[a], He LIN[a], Shuai LU[a,b], Bin WANG[a,b], Kun WANG[c]

[a]*Key Laboratory of Optoelectronic Materials Chemistry and Physics*, *Fujian Institute of Research on the Structure of Matter*, *Chinese Academy of Sciences*, *Fuzhou 350002*, *China*
[b]*University of Chinese Academy of Sciences*, *Beijing 100049*, *China*
[c]*School of Materials Science and Energy Engineering*, *Foshan University*, *Foshan 528000*, *China*

Received: April 30, 2019; Revised: July 11, 2019; Accepted: August 10, 2019

Abstract: A series of YAG:Ce,Mn transparent ceramics were prepared via a solid-state reaction-vacuum sintering method. The effects of various Mn^{2+}–Si^{4+} pair doping levels on the structure, transmittance, and luminescence properties were systematically investigated. These transparent ceramics have average grain sizes of 10–16 μm, clean grain boundaries, and excellent transmittance up to 83.4% at 800 nm. Under the excitation of 460 nm, three obvious emission peaks appear at 533, 590, and 745 nm, which can be assigned to the transition 5d→4f of Ce^{3+} and $^4T_1 \rightarrow {}^6A_1$ of Mn^{2+}. Thus, the Mn^{2+}–Si^{4+} pairs can effectively modulate the emission spectrum by compensating broad orange-red and red spectrum component to yield high quality warm white light. After the optimized YAG:Ce,Mn transparent ceramic packaged with blue light-emitting diode (LED) chips, correlated color temperature (CCT) as low as 3723 K and luminous efficiency (LE) as high as 96.54 lm/W were achieved, implying a very promising candidate for application in white light-emitting diodes (WLEDs) industry.

Keywords: Mn^{2+} red-emitting; YAG:Ce,Mn transparent ceramics; white light-emitting diodes (WLEDs) application; low color temperature

1 Introduction

In recent decades, owing to the merits of high luminous efficiency (LE), energy saving, environmental friendliness, and long persistence, white light-emitting diodes (WLEDs) have become an essential part of our daily life [1–4]. Commercial WLEDs normally utilize 460 nm blue light to excite $Y_3Al_5O_{12}:Ce^{3+}$ (YAG:Ce) yellow phosphor dispersed in epoxy or silicone to generate white light, and then white light was achieved through the combination of yellow and blue light [5,6]. Nonetheless, a variety of disadvantages, such as reduced LE, lower lifetime, the shift of emission color, and corresponding reduced sensory comfort of human eyes, appear due to the poor heat-resistance and thermal conductivity (0.1–0.4 $W \cdot m^{-1} \cdot K^{-1}$) of these organic materials [7–9]. In addition, the low color rendering index (CRI) value and high correlated color temperature (CCT) value of YAG:Ce-based WLEDs can be caused by the lack of red light component [10]. It is reported that high CCT would affect human health, especially be harmful to human eyes, safety [11], and

* Corresponding author.
E-mail: yfzhou@fjirsm.ac.cn

thereby high performance warm WLEDs with good thermal stability and low CCT value should be systematically studied.

Compared to phosphors, YAG transparent ceramics are one of promising fluorescent matrixes in WLEDs application with high thermal stability due to the low thermal expansion coefficient (8.4×10^{-6} K^{-1}) and high thermal conductivity (9–14 $W\cdot m^{-1}\cdot K^{-1}$) [12]. Furthermore, YAG transparent ceramics can be co-doped with rare earth or transition mental ions as activated center in Y^{3+} or Al^{3+} positions. Since the acquisition of warm white light requires the enrichment of red color in YAG:Ce-based WLEDs, co-doped red-activated center can be expected to yield ideal emission [13,14]. Research about introducing Cr^{3+}, Pr^{3+}, or Tb^{3+} ion as red-emitting ions to YAG matrix has been reported [15–17]. A classic example of this was the preparation of YAG:Ce, Pr, Cr transparent ceramic, which possesses high LE of 89.3 lm/W and CRI of 78 by the introduction of red emission band at 609, 638, 677, and 689 nm [15], along with LE of 89 lm/W was achieved by the Ce, Cr co-doped YAG transparent ceramics [16]. Besides, warm white light with a CCT value of ~3000 K and CRI value of 78.9 as well as LE of 38.5–58.9 lm/W was achieved by the transparent ceramics $Gd_3Al_4GaO_{12}:Ce^{3+}$ ($GAGG:Ce^{3+}$) when light-emitting diodes (LEDs) were driven at 350 mA [18]. However, the problem of preparing $GAGG:Ce^{3+}$ ceramics is that Ga volatilizes and decomposes easily in high temperature and vacuum environment, which results in the non-uniform distribution of $GAGG:Ce^{3+}$ ceramics [19]. To prevent the Ga evaporation at high temperature, a complicated two-step sintering method—oxygen sintering and hot isostatic pressing sintering was proposed to prepare the YAGG:Ce transparent ceramics and then increased the cost [20].

Previous research revealed that Mn^{2+} can emit red light in a strong crystal field by the $^4T_1\rightarrow{}^6A_1$ transition [21,22]. Consequently, the Mn^{2+}-doped YAG:Ce phosphors showed the improvement of CRI and CCT performance of WLEDs, through the combination of three emission bands centered at 560, 593, and 745 nm, when it is excited by 460 nm blue light [23,24]. Moreover, the $Y_{3-m-n}Ce_mMn_nAl_{5-n}Si_nO_{12}$ phosphors were also designed by the incorporation of Mn^{2+}–Si^{4+} pairs and then realized color point tuning for white light generation [25]. Similarly, the LE of 119.93 lm/W, internal quantum yield of 81.0%, and CRI value of 73.6 as well as CCT value of 5674 K were achieved in a Mn-doped $Y_3Al_5O_{12}:Ce^{3+}$ single crystal for WLEDs application [26]. However, it is difficult to prepare large-sized YAG:Ce,Mn single crystal for long production cycle and high cost. Furthermore, the $YAG:Ce^{3+},Mn^{2+},Si^{4+}$ phosphors embedded in glass ceramics (PIGs) were also prepared as a chromatically-tunable luminescent material, in which the CCT and LE reach 4954–3753 K and 80.8–60.3 lm/w, respectively [27]. Moreover, $Lu_3Al_5O_{12}$:Mn (LuAG:Mn) transparent ceramics with red-emitting at 600–700 nm have been reported [28]. In summary, optimized emission with low CCT value can be achieved by the strategy of co-doping of Mn^{2+} in $YAG:Ce^{3+}$ system. In comparison to emission band of Pr^{3+} and Cr^{3+}, Mn^{2+} helps to obtain broad orange-red and red emission band, which is beneficial to reach full-luminescence in the visible range. Although the Mn^{2+} ions have been widely used in inorganic luminescent materials, to the best of our knowledge, the Mn^{2+} doped YAG transparent ceramics, as a more efficient fluorescent conversion media for WLEDs application, have not yet been investigated.

In this work, red-emitting YAG:Ce,Mn transparent ceramics with various Mn^{2+}–Si^{4+} pair doping concentration were successfully fabricated via a solid-state reaction sintering method. Mn^{2+} ions were introduced to compensate broad orange-red and red spectrum component and achieve full emission band in the visible range under the excitation of 460 nm. Besides, Si^{4+} ions were introduced to make the charge balance. A combination of X-ray photoelectron spectroscopy (XPS), X-ray diffraction (XRD), scanning electron microscopy (SEM), fluorescent spectrum, lifetime, and transmittance analysis has been carried out to investigate the microstructure and luminescence properties of YAG:Ce,Mn transparent ceramics in detail. Meanwhile, the effects of Mn^{2+}–Si^{4+} pair doping concentration on the structure, transmittance, and luminescence properties, and the energy transfer mechanism were discussed. The YAG:Ce,Mn transparent ceramics assembled with blue LED chips have tunable emission from cold white to warm white as well as high LE and low CCT, which are promising candidates for warm WLEDs application.

2 Experimental

2.1 Sample preparation

$Y_{2.994}Al_{5-2y}O_{12}:0.006Ce^{3+},yMn^{2+},ySi^{4+}$ (y = 0, 0.01, 0.03,

0.06, 0.09, 0.12) (YAG:Ce,Mn) transparent ceramics were prepared by a solid-state reaction sintering method. High-purity commercial powder Al_2O_3 (99.99%), Y_2O_3 (99.99%), CeO_2 (99.95%), MnO (99.95%), and SiO_2 (99.9%) were used as raw materials. Among them, Si^{4+} from SiO_2 was introduced to make the charge balance. 0.05 wt% MgO and 0.5 wt% tetraethyl orthosilicate (TEOS) were used as sintering aids. According to the composition listed in Table 1, raw materials were ball milled for 24 h in ethanol, and then the ethanol slurry was dried at 60 ℃ for 12 h and sieved through a 200-mesh screen. The fine powder was pressed into pellets (Φ = 40 mm) followed by cold isostatic pressed at 200 MPa. After removing the residual organic at 900 ℃ for 8 h, the compacted pellets were sintered at 1750 ℃ for 8 h under vacuum environment. All the samples were polished to 1 mm for characterization. Besides, Mn^{2+} singly doped transparent ceramic $Y_3Al_{4.76}O_{12}$:0.12Mn^{2+}, 0.12Si^{4+} (YAG:Mn) was also prepared as a comparison.

2. 2 Characterization

The crystal structure was characterized by X-ray diffraction (XRD, Miniflex600, Rigaku, Japan) with Cu Kα radiation. Microstructures were observed by field emission scanning electron microscope (FESEM, SU-8010, Hitachi, Japan). In-line transmittance curves were measured using a UV/VIS/NIR spectrophotometer (Lambda950, Perkin Elmer, USA). The valance state of Mn ions was demonstrated via X-ray photoelectron spectroscopy (XPS, Escalab250Xi, Thermo Fisher, USA). Room-temperature photoluminescence (PL) and photoluminescence excitation (PLE) spectra were tested using a fluorescence spectrophotometer (FLS920, Edinburgh Instruments, UK) equipped with a xenon lamp as the excitation source. Fluorescence decay curves were recorded using a fluorescence spectrophotometer (FLS980, Edinburgh Instruments, UK) equipped with 470 nm laser as the excitation source. These transparent ceramics were packaged with commercial 460 nm blue chips into LED chip-on board (COB) modules and further LED lamps in Zhongkexinyuan Photoelectric Technology Co. (Fuzhou, China). The related room-temperature CCT, LE, and Commission International de L'Eclairage (CIE) chromaticity color coordinates of YAG:Ce,Mn transparent ceramics were measured using an integrating sphere (Everfine PMS-50 system, EVERFINE Corporation, Hangzhou, China).

3 Results and discussion

Figure 1 shows the optical pictures of YAG:Ce,Mn transparent ceramics CM0, CM1, CM2, CM3, CM4, and CM5 (y = 0, 0.01, 0.03, 0.06, 0.09, 0.12), respectively. These ceramic samples were double-polished and displayed homogeneous appearance. The size of these samples is 30 mm in diameter and 1.0 mm in thickness, through which the words on back can be seen clearly. After the introduction of more Mn^{2+}–Si^{4+} pairs, YAG:Ce,Mn transparent ceramics' color gradually changes from yellow to red.

Figure 2 shows the XRD patterns of transparent ceramics CM0–CM5 with various Mn^{2+}–Si^{4+} pair concentration. It can be seen from Fig. 2 that diffraction peaks of ceramics CM0–CM3 perfectly match with the standard YAG (PDF#33-0040) phase and no secondary phase is detected, indicating Ce^{3+} and Mn^{2+}–Si^{4+} pairs have been completely incorporated into YAG crystal lattice when y = 0, 0.01, 0.03, and 0.06. However, several weak diffraction peaks aside from the standard YAG phase appear when y = 0.09 and 0.12, indicating that secondary phase exists in ceramics CM4 and CM5. These peaks match with the standard Mg_2SiO_4 (PDF#74-1681) phase. The existence of secondary phase would result in inhomogeneous microstructure. Besides, diffraction peaks slightly shift toward to lower angle

Table 1 Ingredients of $Y_{2.994}Al_{5-2y}O_{12}$:0.006Ce^{3+},yMn^{2+},ySi^{4+} transparent ceramics

Ceramics		Doped			Stoichiometry
		Ce^{3+}	y/Mn^{2+}	y/Si^{4+}	
CM0	YAG:Ce	0.006	0	0	$Y_{2.994}Al_5O_{12}$:0.006Ce
CM1	YAG:Ce,Mn	0.006	0.01	0.01	$Y_{2.994}Al_{4.98}O_{12}$:0.006Ce,0.01Mn^{2+},0.01Si^{4+}
CM2	YAG:Ce,Mn	0.006	0.03	0.03	$Y_{2.994}Al_{4.94}O_{12}$:0.006Ce,0.03Mn^{2+},0.03Si^{4+}
CM3	YAG:Ce,Mn	0.006	0.06	0.06	$Y_{2.994}Al_{4.88}O_{12}$:0.006Ce,0.06Mn^{2+},0.06Si^{4+}
CM4	YAG:Ce,Mn	0.006	0.09	0.09	$Y_{2.994}Al_{4.82}O_{12}$:0.006Ce,0.09Mn^{2+},0.09Si^{4+}
CM5	YAG:Ce,Mn	0.006	0.12	0.12	$Y_{2.994}Al_{4.76}O_{12}$:0.006Ce,0.12Mn^{2+},0.12Si^{4+}

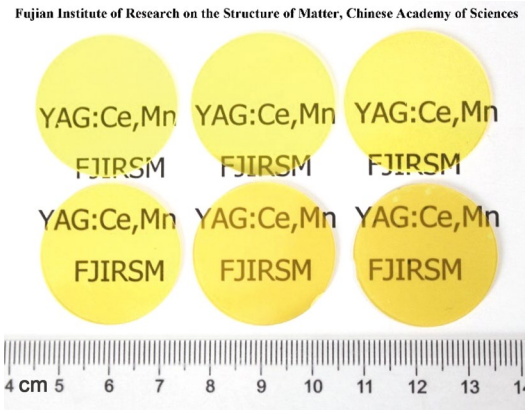

Fig. 1 Photograph of transparent ceramics CM0–CM5.

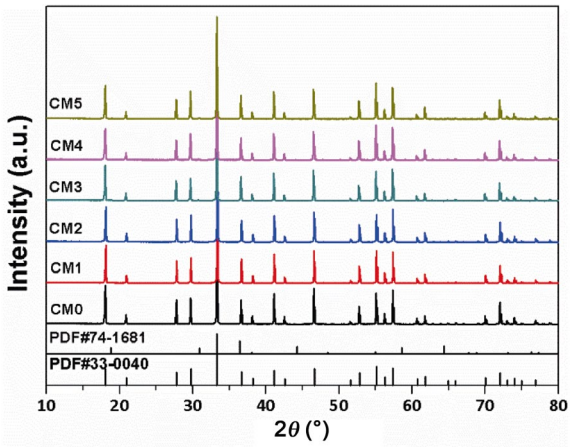

Fig. 2 XRD patterns of standard YAG crystal and ceramics CM0–CM5.

range with increasing Mn^{2+}–Si^{4+} pair concentration, suggesting that YAG:Ce,Mn transparent ceramics obtain expanding unit cell. The expanding unit cell may be attributed to bigger ion size of Ce^{3+} (r = 0.1143 nm) and Mn^{2+} (r = 0.096 nm) in comparison with Y^{3+} (r = 0.1019 nm) and Al^{3+} (r = 0.054 nm), although the ion size of Si^{4+} (r = 0.026 nm) is smaller [15,26].

SEM surface morphologies of YAG:Ce,Mn transparent ceramics via thermal etched method are displayed in Fig. 3. Average grain size of ceramics CM0–CM5 is measured to be 16.4, 15.0, 14.4, 14.0, 11.0, and 10.5 μm, respectively. It is obvious that the addition of Mn^{2+}–Si^{4+} pairs can significantly affect the average grain size of the YAG:Ce,Mn ceramics. Moreover, it can be seen from Figs. 3(a)–3(d) that ceramics CM0–CM3 have regular crystal grains and clean crystal boundaries without obviously secondary phase and residual pores. However, as y = 0.09 and 0.12, grain boundaries of ceramics CM4 and CM5 gradually broaden (Figs. 3(e) and 3(f)). Thus, it can be

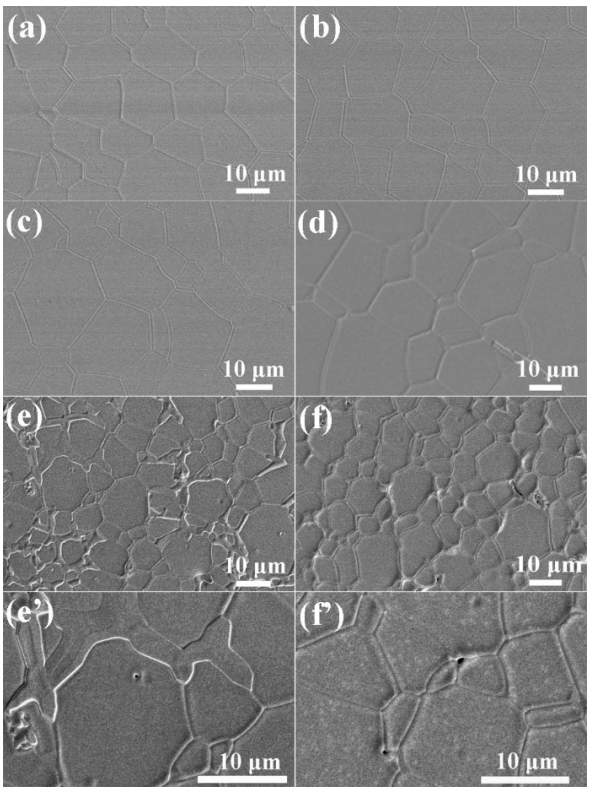

Fig. 3 Thermal etched SEM of surface morphologies: (a) CM0, (b) CM1, (c) CM2, (d) CM3, (e) CM4, (f) CM5, and enlarged views: (e') CM4 and (f') CM5.

reasonably concluded that the coexisting Mg_2SiO_4 forms a liquid phase during the sintering process and is distributed around grain boundaries due to the excess of Si^{4+}. The reason why that grain boundaries broaden and Mg_2SiO_4 phase appears is that SiO_2 may play the dual role of charge balancer and sintering aids, which would cause the deviation in composition from the stoichiometry of YAG:Ce,Mn ceramics. Additional TEOS as sintering aids was introduced; however, redundant Si^{4+} would induce secondary phase formation when y = 0.09 and 0.12. Seriously, residual pores are observed in ceramics CM4 and CM5 (Figs. 3(e) and 3(f)), which would reduce the densification and result in lower transmittance. In order to see clearly grain boundaries and pores, the enlarged view of ceramics CM4 and CM5 are shown in Figs. 3(e') and 3(f'), respectively. One reason why the wider grain boundaries can be seen in Figs. 3(e) and 3(e') is that the thermal corrosion time is too long and residual pores mainly appear in grain boundaries. This result suggests that the Mn^{2+}–Si^{4+} pair doping concentration should be optimized to avoid the existence of pores and impurity phase as well as help to improve the density of YAG:Ce,Mn transparent ceramics.

Figure 4 presents the in-line transmittance spectra of transparent ceramics CM0–CM5 and ceramic M5 (YAG:Mn, $Y_3Al_{4.76}O_{12}$:0.12Mn^{2+},0.12Si^{4+}). On one hand, as shown in Fig. 4(a), ceramics CM0–CM5 obtain extremely high optical transmittance from 300 to 800 nm. The ceramic CM0 obtains best transmittance of 83.4% at 800 nm, which almost reaches the theoretical limit (84%) of YAG transparent ceramics. As Mn^{2+}–Si^{4+} pairs were introduced into the YAG:Ce structure, the transmittance of ceramics CM1, CM2, CM3, CM4, and CM5 reaches 83.3%, 82.5%, 82.3%, 78.4%, and 78.0% at 800 nm, respectively. These results are consistent with SEM results shown in Fig. 3. The lower transmittance of ceramics CM4 and CM5 can be ascribed to inhomogeneous microstructure and residual pores. On the other hand, similar absorption bands around 340 nm and 440–470 nm are observed in ceramics CM0–CM5, which can be attributed to the transition of Ce^{3+} ions from its 4f ground state to 5d excited state [29]. That indicates YAG:Ce,Mn ceramics can be effectively excited under the 460 nm excitation. Nevertheless, the absorption intensity around 340 nm and 440–470 nm gradually declines with increasing Mn^{2+}–Si^{4+} pair doping concentration. That would be related to expanding unit cell in YAG:Ce,Mn ceramics and the energy transfers from Ce^{3+} to Mn^{2+}. Mn^{2+} singly doped transparent ceramic M5 was also prepared via the same process. As shown in Fig. 4(b), the in-line transmittance of 1.0 mm thick ceramic M5 (the inset photo in Fig. 4(b)) is up to 74.3% at 800 nm. No obviously apparent absorption band can be found, especially at 460 nm, indicating that Mn^{2+} is hard to be directly excited by blue light.

Figure 5 shows the XPS spectra of YAG:Ce,Mn ceramics. Figure 5(a) shows the survey scan of XPS, and it indicates the existence of Y, Al, O, Si, and Mn. Figure 5(b) presents the high-resolution XPS spectrum of Mn 2p of ceramic CM5. Two separate peaks with the binding energy of 641.5 and 653.1 eV belong to the Mn $2p_{3/2}$ and Mn $2p_{1/2}$, respectively, with energy difference of 11.6 eV. These values reveal that Mn^{2+} exists in YAG:Ce,Mn ceramic samples, which is consistent with that of Mn^{2+} in $MgY_2Al_4SiO_{12}$:Ce^{3+},Mn^{2+} phosphor [30].

Figure 6 presents the PL and PLE spectra of ceramic CM0, CM5, and M5. The PL spectrum of ceramic

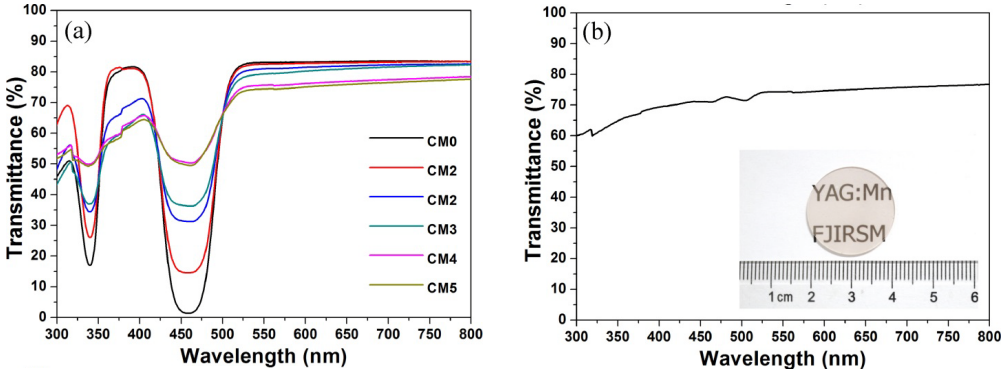

Fig. 4 In-line transmittance spectra: (a) ceramics CM0–CM5 and (b) ceramic M5.

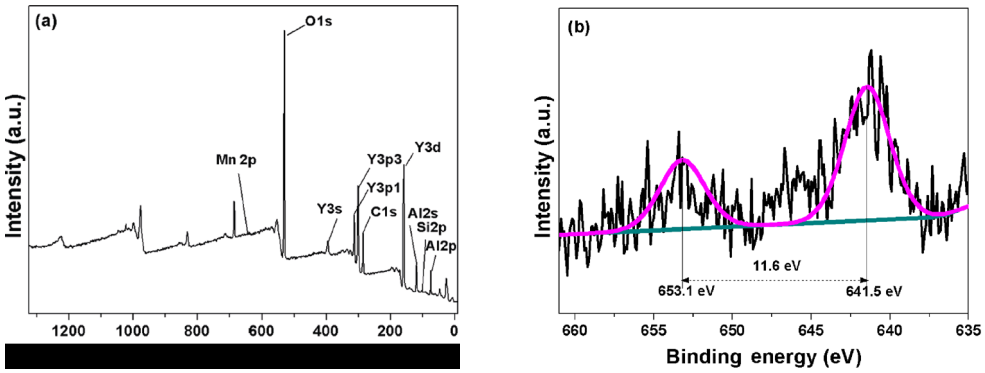

Fig. 5 XPS spectra of YAG:Ce,Mn ceramic: (a) XPS survey scan and (b) Mn 2p.

CM0 exhibits a typical Ce^{3+} yellow-green broad band centered at 533 nm (Fig. 6(a)), which can be attributed to the 5d→4f transition of Ce^{3+} in YAG matrix [5,6,15]. These two excitation bands centered at 340 and 460 nm are corresponding to absorption bands in transmittance spectrum, respectively. And the excitation intensity at 460 nm is stronger than that of 340 nm for the reason that YAG:Ce,Mn ceramics obtain higher absorption for blue light. After Mn^{2+}–Si^{4+} pairs were introduced into the YAG:Ce ceramics, it can be seen from Fig. 6(b) that two obvious emission bands aside from Ce^{3+} emission band are observed at 590 and 745 nm, which is similar to the PL spectrum of Mn^{2+}-doped YAG phosphors and PIGs phosphor [27,28,31]. As for the emission band of Mn^{2+} at 528 nm, its intensity is so weak in comparison to strong Ce^{3+} emission intensity that it cannot be observed. Besides, it is commonly accepted that Mn with different valences emit different luminescence properties. Aside from the aforementioned emission wavelength of Mn^{2+} ions, Mn^{3+} emission bands are observed peaked at 608 and 760 nm attributed to $^5T_2 \rightarrow {}^5E$ transition and Mn^{4+} emission bands are observed peaked at 668 nm attributed to $^2E \rightarrow {}^4A_2$ [26,28]. In this work, the luminescence wavelength of Mn^{3+} and Mn^{4+} can not be observed and it is worth noting that Mn^{2+} is oxidized little or nothing in the vacuum environment, and thus almost Mn^{2+} ions exist in YAG:Ce,Mn transparent ceramics. That is consistent with the XPS results. These PLE spectra of ceramic CM5 monitored at 533, 590, and 745 nm show a similar shape, further supporting the energy transfers from Ce^{3+} to Mn^{2+}. Moreover, several weak bands are observed in PLE spectrum in the wavelength from 300 to 500 nm. Figure 6(c) shows the PL and PLE spectrum of ceramic M5 and its PL spectrum exhibits three emission bands of Mn^{2+} around 528, 590, and 745 nm, further supporting the existence of Mn^{2+} ions. In addition, the same excitation bands centered at 375, 408, 425, 450, and 468 nm are observed via monitored Mn^{2+} emission wavelength at 590 nm, corresponding to transition of $^6A_1(^6S)$ ground state to $^4T_2(^4D)$, [$^4A_1(^4G)$, $^4E(^4G)$], $^4T_2(^4G)$, and $^4T_1(^4G)$ excited state, respectively [23,25,32].

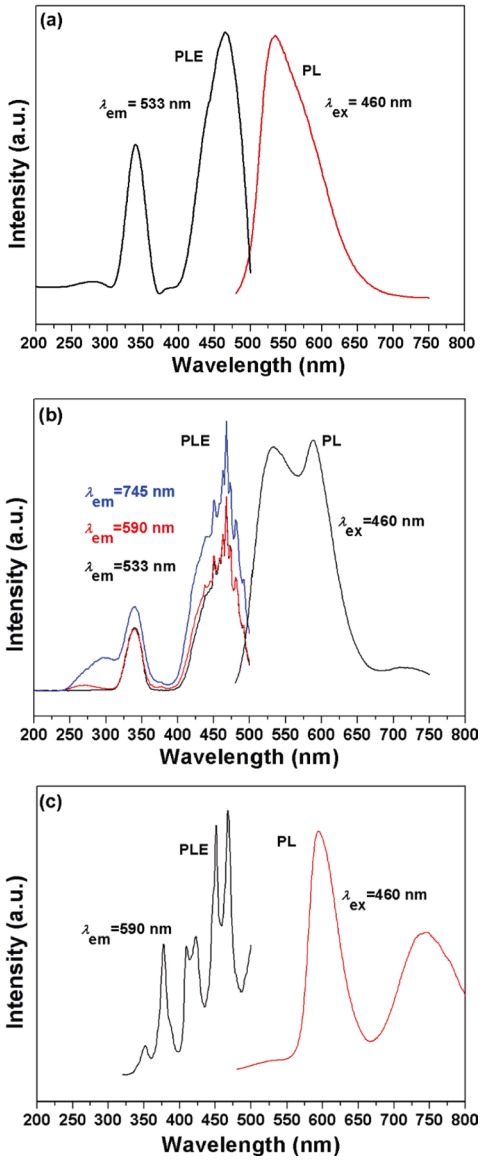

Fig. 6 PL and PLE spectra: (a) ceramic CM0, (b) ceramic CM5, and (c) ceramic M5.

Figure 7 shows the PL spectra of ceramics CM0–CM5. All samples achieve a broad band of Ce^{3+} ions centered at 533 nm under the excitation of 460 nm. After the introduction of Mn^{2+}–Si^{4+} pairs, two emission bands of Mn^{2+} are maximized at 590 and 745 nm. Furthermore, with increasing Mn^{2+}–Si^{4+} pair concentration, the emission intensity of Ce^{3+} declines, but that of

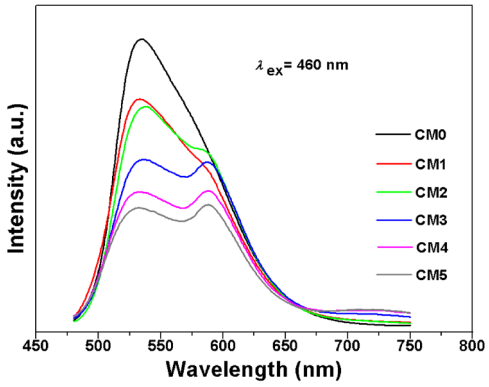

Fig. 7 PL spectra of transparent ceramics CM0–CM5 under 460 nm excitation.

Mn^{2+} increases monotonously. These results are related to the reduced absorption of Ce^{3+} around 440–470 nm with increasing Mn^{2+}–Si^{4+} pair content, which gives strong evidence of the energy transfer from Ce^{3+} to Mn^{2+} ions. Although the doping value y is up to 0.12, the emission intensity of Mn^{2+} at around 745 nm is still weak. It is acknowledged that the wavelength of 745 nm is insensitive to human eyes due to adjacent infrared region. Hence, after optimizing Mn^{2+} doping concentration, the Mn^{2+} doping can enrich red light component and help tune the color point toward red region via emission maximized at 590 nm, which is greatly beneficial to obtain desirable CCT value and then generate warm white light.

Figure 8 presents the fluorescence decay curves of ceramics CM0–CM5. Under 470 nm laser light excitation, decay curves were recorded via monitoring Ce^{3+} emission peak at 533 nm. Their average lifetime of ceramics CM0–CM5 were calculated to be 74, 63, 58, 53, 48, and 46 ns, respectively, and therefore a fluorescence decay process takes place quickly in Ce^{3+} and Mn^{2+}–Si^{4+} pair co-doped system, which reveals the mechanism of energy transfer between Ce^{3+} and Mn^{2+} and it is similar to Ref. [27]. In addition, the energy transfer efficiency (η_T) of $Ce^{3+}\rightarrow Mn^{2+}$ in YAG:Ce,Mn transparent ceramic should be taken into consideration. According to the average lifetime, η_T can be obtained from the formula [25,33]:

$$\eta_T = 1 - \tau/\tau_0 \quad (1)$$

where τ is the average lifetime of the donor Ce^{3+} ions in the presence of the acceptor Mn^{2+} ions and τ_0 is the average lifetime of the donor Ce^{3+} ions without acceptor Mn^{2+} ions. Then, the η_T of various YAG:Ce,Mn transparent ceramics was calculated and listed in Table 2. In this work, the η_T shows an enhancement as the

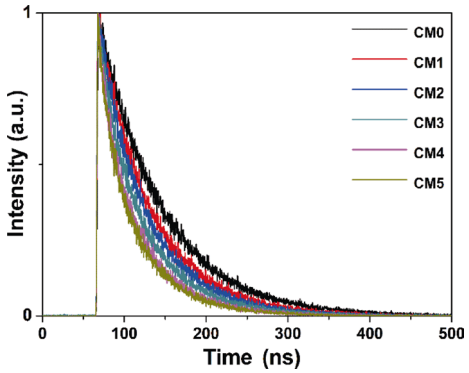

Fig. 8 Fluorescence decay curves of the Ce^{3+} emission peaked at 533 under 470 nm excitation of the ceramics CM0–CM5.

Table 2 Energy transfer efficiency of $Ce^{3+}\rightarrow Mn^{2+}$ in YAG:Ce,Mn transparent ceramics

Mn^{2+} concentration (y)	0	0.01	0.03	0.06	0.09	0.12
Energy transfer efficiency (%)	—	14.8	21.6	28.3	35.1	37.8

increasingly rise of Mn^{2+}–Si^{4+} content and reaches 37.8% when y = 0.12, which reveals the energy transfer from Ce^{3+} to Mn^{2+} ions and results in reduced emission intensity of Ce^{3+} ions as well as increased emission intensity of Mn^{2+} ions.

According to the PL spectra and fluorescence decay curves as well as Refs. [23,26,27], the energy transfer process in YAG:Ce,Mn transparent ceramics can be illustrated as Fig. 9. After Ce^{3+} replaced Y^{3+} position, its 4f ground state splits to $^2F_{5/2}$ and $^2F_{7/2}$ energy level due to spin-coupling. Also, energy splitting of 5d excited state occurs. Under the excitation of 460 nm, the electronic state of Ce^{3+} is excited to upper 5d state. Next, a rapid electron relaxation process takes place from 5d state to $^2F_{5/2}$ and $^2F_{7/2}$ energy level, which emits a broad yellow-green band centered at 533 nm. Because the lowest $5d^1$ energy level of Ce^{3+} is a little higher than the $^4T_1$ of Mn^{2+}, the energy transfer process takes place easily from Ce^{3+} to neighboring Mn^{2+} via non-radiation transition. And then the $^4T_1$ excited electrons transfer back to $^6A_1$ ground state, which emits three bands at 528, 590, and 745 nm since the local environment around the Mn^{2+} ions differ. Such spin-forbidden transition with broad bands would be beneficial for the full emission spectrum in the visible range.

In order to evaluate the illumination performance of these transparent ceramics, ceramics CM0–CM5 were

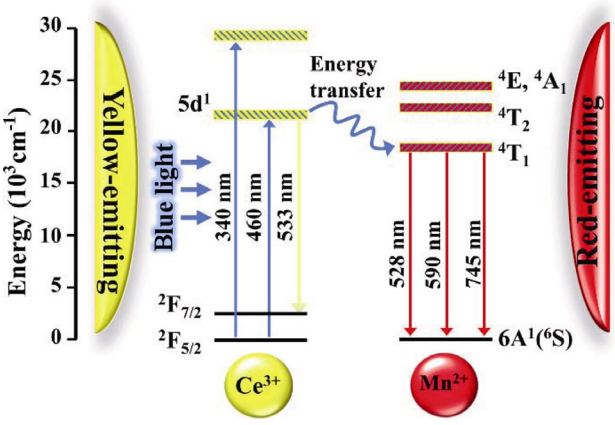

Fig. 9 Schematic illustration of the energy transfer process in the YAG:Ce,Mn transparent ceramics.

combined with commercial blue LED chips. Table 3 shows the value of CCT, LE, and CIE chromaticity color coordinates. Ceramic CM0 shows the highest CCT (4044 K) due to the deficiency of red spectrum, although the LE is the highest. As Mn^{2+}–Si^{4+} pairs were introduced, the CCT and LE simultaneously decrease. Among them, transparent ceramics CM1–CM3 with proper CCT of 3933–3402 K and LE of 103.46–68.79 lm/W are promising fluorescent materials for warm WLEDs application. In comparison to YAG:Ce ceramics, the LE of YAG:Ce,Mn fluorescent ceramics inevitably decreases on account of energy transfer between Ce^{3+} and Mn^{2+}. However, YAG:Ce,Mn ceramics obtain low CCT value and achieve warm white light. That is good for the health of human eyes.

Figure 10(a) shows CIE chromaticity color coordinates diagram of ceramics CM0–CM5 as these transparent ceramics were excited by 460 nm blue light. With increasing Mn^{2+}–Si^{4+} pair doping concentration, their color coordinates ranging from (0.425, 0.552) to (0.474, 0.507) mean emission color can shift from yellow-green to orange and the enrichment of red spectrum component. As a result, it is promising to achieve high quality warm white light via YAG:Ce,Mn ceramics when combined with blue LEDs. Figure 10(b) presents the optical picture of transparent ceramics CM0 and CM2 fabricated in COB modules. After encapsulating lampshade, Fig. 10(c) shows the luminescent result of related turn-on LED lamps. These two LED lamps all emit bright light, but Lamp B based on ceramic CM0 emits cold white light. The high quality warm white light can be obtained from the Lamp A based on ceramic CM2 with CCT of 3723 K and LE of 96.54 lm/W, which is superior to other reported of Ce^{3+} and red activated ion co-doped ceramic-based warm WLEDs.

Table 3 CCT, LE, and CIE chromaticity color coordinates of transparent ceramics CM0–CM5 packaged with LEDs

Ceramics	CCT (K)	LE (lm/W)	Color coordinates (x, y)
CM0	4044	104.91	(0.425, 0.552)
CM1	3933	103.46	(0.430, 0.548)
CM2	3723	96.54	(0.443, 0.537)
CM3	3402	68.79	(0.461, 0.520)
CM4	3256	54.59	(0.469, 0.512)
CM5	3152	39.76	(0.474, 0.507)

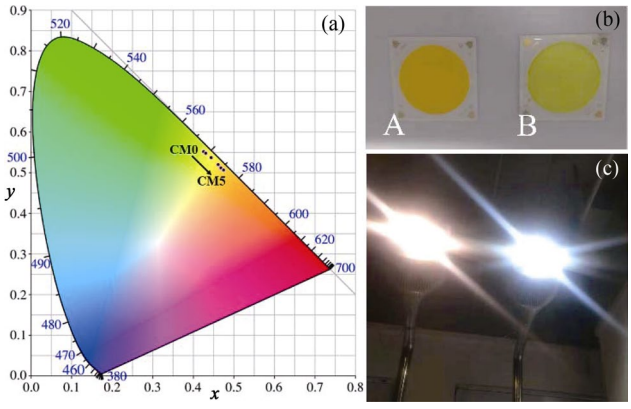

Fig. 10 (a) CIE chromaticity color coordinate diagram for transparent ceramics CM0–CM5 excited by 460 nm blue LED chips, (b) the photo of ceramics CM2 and CM0 LED COB modules, and (c) the photo of related turn-on LED lamps.

4 Conclusions

In summary, YAG:Ce,Mn transparent ceramics with excellent luminescence properties have been successfully prepared. The effects of Mn^{2+}–Si^{4+} pair doping concentration on microstructure, optical, and luminescence properties were systematically discussed. Mn^{2+} ions can enrich red spectrum component via the broad emission bands centered at 590 and 745 nm. The transmittance analysis, PL and PLE spectrum, as well as fluorescence lifetime prove energy transfer from Ce^{3+} to Mn^{2+}. Finally, warm white LED lighting was achieved via optimized Mn^{2+}–Si^{4+} doping. Chromaticity color coordinates of YAG:Ce,Mn ceramics can be varied from (0.425, 0.552) to (0.474, 0.507) by controlling the Mn^{2+}–Si^{4+} doping concentration. The LED light source with high LE (96.54 lm/W) and low CCT (3723 K) was accomplished packaged with YAG:Ce,Mn transparent ceramic CM2 (y = 0.03). The present work demonstrates the promising application of YAG:Ce,Mn transparent ceramics in the field of warm WLEDs. In order to improve the LE of YAG:Ce,Mn packaged LED, the introduction of Al_2O_3 scattering centers is an excellent strategy and the related work is on-going.

Acknowledgements

This work was supported by the CAS Priority Research program (XDB20010300, XDA21010204), National Natural Science Foundation of China (201501178), and Natural Science Foundation of Fujian Province (2017H0048).

References

[1] Nishiura S, Tanabe S, Fujioka K, *et al*. Preparation and optical properties of transparent Ce: YAG ceramics for high power white LED. *IOP Conf Ser: Mater Sci Eng* 2009, **1**: 012031.

[2] Chen ZH, Li JT, Xu JJ, *et al*. Fabrication of YAG transparent ceramics by two-step sintering. *Ceram Int* 2008, **34**: 1709–1712.

[3] Samuel P, Kumar GA, Takagimi Y, *et al*. Efficient energy transfer between Ce^{3+}/Cr^{3+} and Nd^{3+} ions in transparent Nd/Ce/Cr: YAG ceramics. *Opt Mater* 2011, **34**: 303–307.

[4] Lin ZB, Lin H, Xu J, *et al*. Highly thermal-stable warm w-LED based on Ce: YAG PiG stacked with a red phosphor layer. *J Alloys Compd* 2015, **649**: 661–665.

[5] Hu S, Lu CH, Zhou GH, *et al*. Transparent YAG: Ce ceramics for WLEDs with high CRI: Ce^{3+} concentration and sample thickness effects. *Ceram Int* 2016, **42**: 6935–6941.

[6] Liu GH, Zhou ZZ, Shi Y, *et al*. Ce: YAG transparent ceramics for applications of high power LEDs: Thickness effects and high temperature performance. *Mater Lett* 2015, **139**: 480–482.

[7] Nishiura S, Tanabe S, Fujioka K, *et al*. Properties of transparent Ce: YAG ceramic phosphors for white LED. *Opt Mater* 2011, **33**: 688–691.

[8] Yun S, Wu LX, Chen H, *et al*. Study of Ce: $Y_3Al_5O_{12}$ transparent ceramics for application of white light emiting diode. *Laser Optoelectron Prog* 2014, **51**: 052302.

[9] Lin H, Hu T, Cheng Y, *et al*. Glass ceramic phosphors: Towards long-lifetime high-power white light-emitting-diode applications-A review. *Laser Photonics Rev* 2018, **12**: 1700344.

[10] Yi XZ, Zhou SM, Chen C, *et al*. Fabrication of Ce: YAG, Ce, Cr: YAG and Ce: YAG/Ce, Cr: YAG dual-layered composite phosphor ceramics for the application of white LEDs. *Ceram Int* 2014, **40**: 7043–7047.

[11] Zhang MH, Chen Y, He GX. Color temperature tunable white-light LED cluster with extrahigh color rendering index. *Sci World J* 2014, **2014**: 1–6.

[12] Li SX, Zhu QQ, Tang DM, *et al*. Al_2O_3–YAG: Ce composite phosphor ceramic: A thermally robust and efficient color converter for solid state laser lighting. *J Mater Chem C* 2016, **4**: 8648–8654.

[13] Yang H, Kim YS. Energy transfer-based spectral properties of Tb-, Pr-, or Sm-codoped YAG: Ce nanocrystalline phosphors. *J Lumin* 2008, **128**: 1570–1576.

[14] Lin YS, Cheng TC, Tsai CC, *et al*. High-luminance white-light point source using Ce, Sm : YAG double-clad crystal fiber. *IEEE Photon Technol Lett* 2010, **22**: 1494–1496.

[15] Feng SW, Qin HM, Wu GQ, *et al*. Spectrum regulation of YAG: Ce transparent ceramics with Pr, Cr doping for white light emitting diodes application. *J Eur Ceram Soc* 2017, **37**: 3403–3409.

[16] Tang YR, Zhou SM, Yi XZ, *et al*. The Cr-doping effect on white light emitting properties of Ce: YAG phosphor ceramics. *J Am Ceram Soc* 2017, **100**: 2590–2595.

[17] Mu ZF, Hu YH, Wu HY, *et al*. Luminescence and energy transfer of Mn^{2+} and Tb^{3+} in $Y_3Al_5O_{12}$ phosphors. *J Alloys Compd* 2011, **509**: 6476–6480.

[18] Liu S, Sun P, Liu YF, *et al*. Warm white light with a high color-rendering index from a single $Gd_3Al_4GaO_{12}$: Ce^{3+} transparent ceramic for high-power LEDs and LDs. *ACS Appl Mater Interfaces* 2019, **11**: 2130–2139.

[19] Hellstrom EE, Ray RD, Zhang C. Preparation of gadolinium gallium garnet [$Gd_3Ga_5O_{12}$] by solid-state reaction of the oxides. *J Am Ceram Soc* 1989, **72**: 1376–1381.

[20] Hua H, Feng S, Ouyang Z, *et al.* YAGG:Ce transparent ceramics with high luminous efficiency for solid-state lighting application. *J Adv Ceram* 2019, **8**: 389–398.

[21] Palumbo DT, Brown JJ. Electronic states of Mn^{2+}-activated phosphors. *J Electrochem Soc* 1971, **118**: 1159.

[22] Li GG, Xu XG, Peng C, *et al*. Yellow-emitting $NaCaPO_4$: Mn^{2+} phosphor for field emission displays. *Opt Express* 2011, **19**: 16423.

[23] Shi YR, Wang YH, Wen Y, *et al*. Tunable luminescence $Y_3Al_5O_{12}$: 006Ce^{3+}, *x*Mn^{2+} phosphors with different charge compensators for warm white light emitting diodes. *Opt Express* 2012, **20**: 21656.

[24] Wang XJ, Jia DD, Yen WM. Mn^{2+} activated green, yellow, and red long persistent phosphors. *J Lumin* 2003, **102–103**: 34–37.

[25] Jia YC, Huang YJ, Zheng YH, *et al*. Color point tuning of $Y_3Al_5O_{12}$: Ce^{3+} phosphor via Mn^{2+}–Si^{4+} incorporation for white light generation. *J Mater Chem* 2012, **22**: 15146.

[26] Gu GR, Xiang WD, Yang C, *et al*. Synthesis and luminescence properties of a H_2 annealed Mn-doped $Y_3Al_5O_{12}$: Ce^{3+} single crystal for WLEDs. *CrystEngComm* 2015, **17**: 4554–4561.

[27] Chen H, Lin H, Xu J, *et al*. Chromaticity-tunable phosphor-in-glass for long-lifetime high-power warm w-LEDs. *J Mater Chem C* 2015, **3**: 8080–8089.

[28] Zhang YL, Hu S, Liu YL, *et al*. Red-emitting $Lu_3Al_5O_{12}$: Mn transparent ceramic phosphors: Valence state evolution studies of Mn ions. *Ceram Int* 2018, **44**: 23259–23262.

[29] Jang HS, Im WB, Lee DC, *et al*. Enhancement of red spectral emission intensity of $Y_3Al_5O_{12}$: Ce^{3+} phosphor via Pr co-doping and Tb substitution for the application to white LEDs. *J Lumin* 2007, **126**: 371–377.

[30] Pan ZF, Chen JC, Wu HQ, *et al*. Red emission enhancement in Ce^{3+}/Mn^{2+} co-doping suited garnet host $MgY_2Al_4SiO_{12}$ for tunable warm white LED. *Opt Mater* 2017, **72**: 257–264.

[31] Chen DQ, Zhou Y, Xu W, *et al*. Enhanced luminescence of Mn^{4+}: $Y_3Al_5O_{12}$ red phosphor via impurity doping. *J Mater Chem C* 2016, **4**: 1704–1712.

[32] Chang CK, Chen TM. White light generation under violet-blue excitation from tunable green-to-red emitting $Ca_2MgSi_2O_7$: Eu, Mn through energy transfer. *Appl Phys Lett* 2007, **90**: 161901.

[33] Song YH, Jia G, Yang M, *et al*. $Sr_3Al_2O_5Cl_2$: Ce^{3+}, Eu^{2+}: A potential tunable yellow-to-white-emitting phosphor for ultraviolet light emitting diodes. *Appl Phys Lett* 2009, **94**: 091902.